Synthesis and Characterization of a New Family of Thermally Stable Open-Framework Zincophosphate/Arsenate Phases: $M_3Zn_4O(XO_4)_3 \cdot nH_2O$ (M = Na, K, Rb, Li, ...; X = P, As; n = ∼3.5−6). Crystal Structures of $Rb_3Zn_4O(PO_4)_3 \cdot 3.5H_2O$, $K_3Zn_4O(AsO_4)_3 \cdot 4H_2O$, and $Na_3Zn_4O(PO_4)_3 \cdot 6H_2O$

William T. A. Harrison*

Department of Chemistry, University of Western Australia, Nedlands, WA 6907, Australia

Robert W. Broach and Robert A. Bedard

UOP Research Center, 50 East Algonquin Road, Des Plaines, Illinois 60017

Thurman E. Gier, Xianhui Bu, and Galen D. Stucky

Department of Chemistry, University of California, Santa Barbara, California 93106-9510

Received July 25, 1995. Revised Manuscript Received December 15, 1995[⊗]

The syntheses, representative crystal structures, and some properties of a new family of microporous zincophosphate/arsenate materials, denoted $M_3Zn_4O(XO_4)_3 \cdot nH_2O$ (M = Li, Na, K, Rb, Cs, ...; X = P, As; n = ∼3.5−6), are reported. All these materials are based on a flexible, anionic $Zn_4O(XO_4)_3$ network built up from vertex-linked tetrahedral ZnO_4 and XO_4 units. Four ZnO_4 units share a vertex, resulting in novel OZn_4 centers. The use of mixed four-coordinate anion types (XO_4^{3-}, O^{2-}) results in a number of interesting structural and stability properties. The $M_3Zn_4O(XO_4)_3 \cdot nH_2O$ network contains only pairs of 3-rings (a spiro-5 unit) and 8-rings, and no 4-rings or 6-rings: it encloses roughly spherical cavities connected by a three-dimensional network of 8-ring channels propagating in the orthogonal [100], [010], and [001] directions (cubic unit-cell axes). Extraframework cations and water molecules occupy these cavities and channels. These phases display typical "zeolitic" dehydration/rehydration and ion-exchange reactions with thermal stabilities up to 600 °C, the highest known for this type of open-framework Zn(P/As)O material. The included guest cation (Na, Rb, K, Li, ...) has a crucial effect on crystal structure, by ordering in and modifying the configuration of the intercavity 8-ring channels. The crystal structures of $Rb_3Zn_4O(PO_4)_3 \cdot 3.5H_2O$, $K_3Zn_4O(AsO_4)_3 \cdot 4H_2O$, and $Na_3Zn_4O(PO_4)_3 \cdot 6H_2O$ are presented. Crystal data: $Rb_3Zn_4O(PO_4)_3 \cdot 3.5H_2O$, M_r = 881.40, cubic, space group $F\bar{4}3c$ (No. 219), a = 15.3423(9) Å, V = 3611.4(6) Å^3, Z = 8, R_p = 5.12%, R_{wp} = 6.78%, 27 parameters, 1874 data points (X-ray Rietveld refinement). $K_3Zn_4O(AsO_4)_3 \cdot 4H_2O$, M_r = 883.63, cubic, space group $F\bar{4}3c$ (No. 219), a = 15.4638(2) Å, V = 3697.9(2) Å^3, Z = 8, R_p = 8.69%, R_{wp} = 11.42%, 24 parameters, 2124 data points (X-ray Rietveld refinement). $Na_3Zn_4O(PO_4)_3 \cdot 6H_2O$, M_r = 739.49, trigonal, space group $R3c$ (No. 161), a = 10.7489(3) Å, α = 60.114(2)°, V = 880.4(4) Å^3, Z = 2, R = 2.49%, R_w = 2.61%, 180 parameters, 846 observed reflections with $I > 3\sigma(I)$ (single-crystal data).

Introduction

Microporous aluminosilicates (zeolites) have been of interest to the academic and industrial communities for many years. With the discovery that open-framework aluminophosphate frameworks analogous to but not necessarily isostructural to zeolite frameworks could be prepared,[1] interest in this relatively mature field has revived, and a very large number of novel open-framework structures have been reported in the past few years.[2] Our own work has focused on the group 2/12/15 (beryllo/zinco)(phosphate/arsenate) (Zn,Be)(P, As)O structure field, in which tetrahedral Be or Zn atoms, in company with P or As, linked (via oxygen-atom bridges, form anionic, three-dimensional networks, leading to new zeolite-like[3−6] and nonzeolitic[7−9] open-framework phases.

We initially reported the existence of a hydrated sodium zinc phosphate with a powder pattern that

[⊗] Abstract published in *Advance ACS Abstracts,* February 1, 1996.

(1) Wilson, S. T.; Lok, B. M.; Messina, C. A.; Cannan, T. R.; Flanigen, E. M. *J. Am. Chem. Soc.* **1982**, *104*, 1146.

(2) (a) Estermann, M.; McCusker, L. B.; Merrouche, A.; Baerlocher, Ch.; Kessler, H. *Nature (London)* **1991**, *352*, 320. (b) Harvey, G.; Meier, W. M. *Zeolites: Facts, Figures, Future: Studies in Surface Science and Catalysis*; Elsevier: Amsterdam, 1989; Vol. 49, p 411. (c) Haushalter, R. C.; Strohmaier, K. G.; Lai, F. W. *Science (Washington, D.C.)* **1989**, *246*, 1289. (d) Soghomonian, V.; Chen, Q.; Haushalter, R. C.; Zubieta, J. *Angew. Chem., Int. Ed. Engl.* **1993**, *32*, 610. (e) Loiseau, T.; Férey, G. *J. Solid State Chem.* **1994**, *111*, 416. (f) Harrison, W. T. A.; Gier, T. E.; Stucky, G. D. *Angew. Chem., Int. Ed. Engl.* **1993**, *32*, 724. (g) Chen, J.; Jones, R. H.; Natrajan, S.; Hursthouse, M. B.; Thomas, J. M. *Angew. Chem., Int. Ed. Engl.* **1994**, *33*, 639. (h) Chippindale, A. M.; Walton, R. I. *J. Chem. Soc., Chem. Commun.* **1994**, 2453.

(3) Gier, T. E.; Stucky, G. D. *Nature (London)* **1991**, *349*, 508.

(4) Harrison, W. T. A.; Gier, T. E.; Moran, K. L.; Nicol, J. M.; Eckert, H.; Stucky, G. D. *Chem. Mater.* **1991**, *3*, 27.

0897-4756/96/2808-0691$12.00/0

indexed excellently on a face-centered cubic cell edge of ~15.2 Å.[10] We have now determined the crystal structure of this material, $Na_3Zn_4O(PO_4)_3 \cdot 6H_2O$, and prepared several analogues. In this paper we report some preliminary synthetic, structural, and physical characterizations of what has turned out to be an extensive new family of novel open-framework zincophosphate/arsenate materials. These phases are built up from ZnO_4 and PO_4/AsO_4 subunits, and because of the connectivity of these units, also contain the unusual OZn_4 unit as a *tetrahedral, oxygen-atom-centered* building unit. The use of mixed anion types (phosphate/arsenate and "oxide") in a molecular sieve structure is a new synthetic approach to control framework charge, pore dimensions, and thermal stability in open framework zincophosphate/arsenates.

The $Na_3Zn_4O(PO_4)_3 \cdot 6H_2O$ structure eventually proved to be rhombohedral. We describe our crystallographic studies on this material in some detail to illustrate some of the pitfalls and advantages of both single-crystal and powder diffraction methods in studying these types of materials. As will be shown below, these new $M_3Zn_4O(XO_4)_3 \cdot nH_2O$ materials are closely related to the pharmacosiderite family of microporous octahedral/tetrahedral networks,[11,12] exemplified by $KFe_4(OH)_4(AsO_4)_3 \cdot \sim 6H_2O$[11] (octahedral/tetrahedral FeO_6/AsO_4 network).

Experimental Section

Synthesis and Initial Characterization. *$Na_3Zn_4O(PO_4)_3 \cdot 6H_2O$:* Clear, cuboidal crystals of this phase were grown by preparing 13 cm^3 of an aqueous solution 0.05 M in $Zn(NO_3)_2$ and 1.15 M in H_3PO_4 in a small polypropylene bottle, and adding 7.5 cm^3 of 4 M NaOH. The initial gel converted to a sludge and then a milk on vigorous shaking (pH = 12.5). After aging for 9 days at 70 °C, the product was recovered by standard vacuum filtration and drying techniques to yield transparent cubes up to 0.5 mm in size, easily separable from a minor phase of cocrystallizing microneedle spherulites of hexagonal $NaZnPO_4 \cdot H_2O$ [a = 10.4797(8) Å, c = 15.089(2) Å, V = 1453 $Å^3$, space group $P6_122$]. Further details of this novel chiral phase are reported elsewhere.[13] Pure $Na_3Zn_4O(PO_4)_3 \cdot 6H_2O$ can be prepared as a powder from a more dilute synthesis with shorter aging, indicating the importance of kinetic control in microporous ZnPO syntheses. The X-ray powder pattern (experimental details given below) indexed cleanly as face-centered cubic (FCC), with a = 15.201(2) Å (V = 3513 $Å^3$). As will be described below, the crystal structure of $Na_3Zn_4O(PO_4)_3 \cdot 6H_2O$ is actually rhombohedral (pseudocubic).

Thermogravimetric analysis (TGA) on $Na_3Zn_4O(PO_4)_3 \cdot 6H_2O$ indicated that the powder lost about 12 wt % at ~160 °C, equivalent to about 4.9 water molecules/$Na_3Zn_4O(PO_4)_3$ formula unit. Assuming 6.0 water molecules in the formula, the calculated weight loss would be 14.6%. The powder second harmonic generation[14] (PSHG) response of $Na_3Zn_4O(PO_4)_3 \cdot 6H_2O$ exhibited a weak but definitely nonzero response (~1 times that of quartz), indicating that the material crystallizes in a noncentrosymmetric space group. So far, the zincoarsenate analogue of $Na_3Zn_4O(PO_4)_3 \cdot 6H_2O$ has resisted synthesis, at least while using sodium as the countercation.

$K_3Zn_4O(PO_4)_3 \cdot 4H_2O$: The potassium analogue of $Na_3Zn_4O(PO_4)_3 \cdot 6H_2O$ was prepared as a fine white powder on a large scale by dissolving 24.36 g of K_2HPO_4 and 10.76 g of 85% KOH pellets in 500 cm^3 of water. To this clear solution was added a solution of 35.7 g of $Zn(NO_3)_2$ in 500 cm^3 of water, and the resulting gel was shaken to homogenize the mixture. After aging at 70 °C for 5 h, 22.3 g of $K_3Zn_4O(PO_4)_3 \cdot 4H_2O$ powder (yield 99%) was recovered by filtration and drying. The powder diffraction pattern indexed as *primitive* cubic, a = 15.189(2) Å (V = 3505 $Å^3$). A combined TGA/DTA trace indicated complete water loss at 300 °C (obs 9%, calc 9.6%, based on four water molecules) with structure retention; at 500 °C, recrystallization to ZnO and $KZnPO_4$ had occurred (X-ray diffraction patterns of residues). The observed PSHG response of $K_3Zn_4O(PO_4)_3 \cdot 4H_2O$ was small but definitely nonzero.

$K_3Zn_4O(AsO_4)_3 \cdot 4H_2O$. This analogue was made by mixing 26 cm^3 of a solution 1.08 M in H_3AsO_4 and 3.65 M in KOH with 12 cm^3 of 2 M $Zn(NO_3)_2$ solution. After aging (14 h at 70 °C), the initial milk was well settled and was recovered by vacuum filtration and drying. The microcrystalline white powder exhibited a diffraction pattern indexable as FCC, a = 15.446(2) Å, V = 3685 $Å^3$. The TGA data showed complete water loss at 300 °C (obs 7.8%, calc 8.2% assuming four water molecules) with structure retention, and the PSHG signal was small but definite (~1 times that of quartz).

$Rb_3Zn_4O(PO_4)_3 \cdot 3.5H_2O$: The cubic Rb-containing modification was prepared as a fine white powder by adding 6.15 g of 50% RbOH to 13 cm^3 of a solution 0.46 M in Zn^{2+} and 1.15 M in H_3PO_4. The initial gel transformed to a milk which settled on aging (1−3 days) at 70 °C. The resulting diffraction pattern indexed as face-centered cubic, with a = 15.327(2) Å (V = 3601 $Å^3$). TGA showed a 7.8% weight loss at ~250 °C, corresponding to ~3.5 water molecules/$Rb_3Zn_4O(PO_4)_3$ unit, see below). The framework is stable to at least 450 °C (X-ray diffraction measurements of post-TGA residue).

The tetragonal form of $Rb_3Zn_4O(PO_4)_3 \cdot 3.5H_2O$ was prepared under slightly more basic conditions (8.61 g of RbOH solution) than the synthesis of cubic $Rb_3Zn_4O(PO_4)_3 \cdot 3.5H_2O$. The recovered white powder had a distinctly different powder patten which indexed as primitive tetragonal with a = 10.931(3) Å and c = 7.623(2) Å (V = 910.8 $Å^3$), i.e., $a \approx a_{cub}/\sqrt{2}$, $c \approx a_{cub}/2$ (a_{cub} = cubic $Rb_3Zn_4O(PO_4)_3 \cdot 3.5H_2O$ cell parameter). TGA for the tetragonal form of $Rb_3Zn_4O(PO_4)_3 \cdot 3.5H_2O$ showed a small but distinct "step" at 70 °C, followed by a 7.8% loss at 250 °C, similar to the weight loss for cubic $Rb_3Zn_4O(PO_4)_3 \cdot 3.5H_2O$. The tetragonal $Rb_3Zn_4O(PO_4)_3 \cdot 3.5H_2O$ structure is stable to at least 450 °C, although it is unknown at present whether it transforms to the cubic variant of $Rb_3Zn_4O(PO_4)_3 \cdot 3.5H_2O$ on thermal treatment.

$Rb_3Zn_4O(AsO_4)_3 \cdot 4H_2O$: Only the cubic form of this analogue has been made, by holding a mixture of 4.04 g of 4 M H_3AsO_4, 8.61 g of 50% RbOH, and 7.68 g of $Zn(NO_3)_2$ at 200 °C for 5 days in a sealed Teflon pouch in an autoclave. The recovered white powder indexed cleanly as FCC, a = 15.610(2) Å (V = 3804 $Å^3$). A small PSHG signal indicated a noncentrosymmetric space group for $Rb_3Zn_4O(AsO_4)_3 \cdot 4H_2O$.

$Cs_3Zn_4O(PO_4)_3 \cdot 4H_2O$: The cesium analogue was made hydrothermally in the tetragonal form only by mixing 3.86 g of 2 M $Zn(NO_3)_2$, 2.39 g of 4 M H_3PO_4, 8 cm^3 of water and 9.0 g of 50% CsOH. After aging overnight at 70 °C, the gel was completely settled. The resulting white powder gave a primitive tetragonal powder pattern, with a = 11.074(3) Å, c = 7.750(2) Å, and V = 950.4 $Å^3$ and exhibited a PSHG signal several times that of quartz.

$Cs_3Zn_4O(AsO_4)_3 \cdot 4H_2O$: This material was made in a fashion similar to that for the phosphate, but by substituting 2.70 g of 4 M H_3AsO_4 for the phosphoric acid (X-ray powder data:

(5) Nenoff, T. M.; Harrison, W. T. A.; Gier, T. E.; Stucky, G. D. *J. Am. Chem. Soc.* **1991**, *113*, 378.
(6) Gier, T. E.; Harrison, W. T. A.; Stucky, G. D. *Angew. Chem., Int. Ed. Engl.* **1991**, *103*, 1191.
(7) Harrison, W. T. A.; Gier, T. E.; Stucky, G. D. *J. Mater. Chem.* **1991**, *1*, 153.
(8) Harrison, W. T. A.; Martin, T. E.; Gier, T. E.; Stucky, G. D. *J. Mater. Chem.* **1992**, *2*, 175.
(9) Harrison, W. T. A.; Nenoff, T. M.; Eddy, M. M.; Martin, T. E.; Stucky, G. D. *J. Mater. Chem.* **1992**, *2*, 1127.
(10) Gier, T. E.; Harrison, W. T. A.; Nenoff, T. M.; Stucky, G. D. *Synthesis of Microporous Materials*; Van Nostrand Reinhold: New York, 1992; Vol. 1, p 407. Gier, T. E. United States Patent 5,152,972.
(11) Buerger, M. J.; Dollase, W. A.; Garaycochea-Wittke, I. *Z. Kristallogr.* **1967**, *125*, 92.
(12) Harrison, W. T. A.; Gier, T. E.; Stucky, G. D. *Zeolites* **1995**, *15*, 408.
(13) Harrison, W. T. A.; Gier, T. E.; Stucky, G. D.; Broach, R. W.; Bedard, R. A. *Chem. Mater.* **1996**, *8*, 145.
(14) Dougherty, J. P.; Kurtz, S. K. *J. Appl. Crystallogr.* **1976**, *9*, 145.

tetragonal, $a = 11.309(3)$ Å, $c = 7.919(2)$ Å, $V = 1013$ Å^3). The TGA trace showed 6.4% water loss to 200 °C; X-ray residue measurements indicated that the framework was stable to 600 °C.

Ion-exchange reactions: Since lithium phosphate is relatively insoluble under the typical pH conditions of the syntheses reported above, the Li-containing $M_3Zn_4O(XO_4)_3 \cdot nH_2O$ analogues could be prepared only by a postiori ion exchange. For example, exchanging the cubic potassium zinc phosphate, $K_3Zn_4O(PO_4)_3 \cdot 4H_2O$, with 5 N LiCl (pH adjusted to 11 with LiOH) overnight at 25 °C, gave $Li_3Zn_4O(PO_4)_3 \cdot 6H_2O$, with a distinctive rhombohedrally distorted powder pattern, compared to the typical ~15.2 Å FCC structure. All the observed lines could be indexed based on a rhombohedral cell with $a = 10.989(4)$ Å, $\alpha = 56.96(1)°$, and $V = 872$ Å^3 (*R*-centered hexagonal setting: $a = 10.482(2)$, $c = 27.481(3)$ Å, $V = 2615$ Å^3). $Li_3Zn_4O(PO_4)_3 \cdot 6H_2O$ probably crystallizes as an isostructure of $Na_3Zn_4O(PO_4)_3 \cdot 6H_2O$ (vide infra).

A similar ion-exchange reaction of the potassium zinc arsenate analogue with LiCl yielded an orthorhombically distorted structure, with $a \approx 10.66$ Å, $b \approx 15.49$ Å, and $c \approx 9.96$ Å ($V \approx 1645$ Å^3). Unlike the parent potassium phase, the Li derivative loses water in two steps: 7.5% to 200 °C, then another 2.5% from 225−300 °C. The structure is stable to dehydration at 200 °C but not at 300 °C. Thermal treatment to 400 °C resulted in an amorphous residue (powder X-ray diffraction), but further heating to 750 °C resulted in recrystallization to a mixture of the stable, condensed phenakite-type $LiZnAsO_4$ and ZnO.

Characterization Techniques. Preliminary X-ray powder data (Scintag automated PAD-X diffractometer, $\theta-\theta$ geometry, flat plate sample, Cu Kα radiation, $\bar{\lambda} = 1.541\,78$ Å, $T = 25(2)$ °C) were collected for the various samples described above.

The powder patterns of most of the above phases could be successfully indexed on face-centered cubic cells, with a ≈ 15.2 Å, double the cubic cell parameter found in the initial single-crystal measurements on $Na_3Zn_4O(PO_4)_3 \cdot 6H_2O$ (vide infra). Some phases showed distortions from the basic 15.2 Å cubic cell, and least-squares fits, based on the Cu Kα_1 peak position ($\lambda = 1.540\,568$ Å) as obtained through a software "stripping" routine, yielded the refined lattice parameters noted above.

Thermogravimetric analyses were performed on a Du Pont 9900 system. Analysis of the TGA data for most of these structures suggested an average water content of ~4.0 per formula unit, and for convenience it is expressed as such in the formulas reported here in the cases where structural information is as yet unavailable. Powder second-harmonic generation (PSHG) measurements were made as described previously,[15] following the method of Dougherty and Kurtz.[14]

Initial Single-Crystal Study of $Na_3Zn_4O(PO_4)_3 \cdot 6H_2O$. A cuboidal crystal of $Na_3Zn_4O(PO_4)_3 \cdot 6H_2O$ (transparent; edge dimension ~0.03 mm) was selected for data collection on a Huber automated diffractometer (graphite-monochromated Mo Kα radiation: $\lambda = 0.710\,73$ Å; room temperature). A cubic unit cell ($a = 7.5999(8)$ Å) was established from reflections found by "black-box" search and indexing routines. The superlattice peaks visible in the X-ray powder data (vide infra) were apparently too weak to be observed for the small crystal studied, and data were collected on the basis of the 7.6 Å subcell. Intensity data ($0 \rightarrow h$, $0 \rightarrow k$, $0 \rightarrow l$) were collected in the $\theta-2\theta$ scanning mode for $0 < 2\theta < 55°$ with three standard reflections monitored every 100 observations for intensity variation throughout the course of the experiment: less than 2% intensity variation was observed. Due to the small crystal size, absorption was assumed to be negligible, and no corrections were made. The raw intensities were reduced to F and $\sigma(F)$ values using a profile-fitting routine,[16] and the normal corrections for Lorentz and polarization effects were made.

There were no systematic absences in the reduced data, comparable with space groups $P23$, $Pm\bar{3}$, $P432$, $P\bar{4}3m$, and $Pm\bar{3}m$. Due to the nonzero PSHG response of $Na_3Zn_4O(PO_3)_3 \cdot 6H_2O$, the centrosymmetric space groups were rejected from further consideration. The gross structural details of $Na_3Zn_4O(PO_4)_3 \cdot 6H_2O$ were established in space group $P\bar{4}3m$ (No. 215): Starting atomic positions for Zn and P were obtained from the direct-methods program SHELXS-86,[17] and the other atomic species were progressively located from Fourier difference maps (software: CRYSTALS[18]). A chemically reasonable structural model resulted, consisting of a zincophophate framework surrounding channels containing guest sodium cations or oxygen atom (water molecule) species. However, upon anisotropic refinement, the thermal parameters of the oxygen atom that forms an intertetrahedral Zn−O−P bridge (vide infra) refined to very large, anisotropic values, and those of the guest species were unstable, indicating to us that the assumption of primitive-cubic symmetry with $a \approx 7.6$ Å was probably incorrect, and the final residuals were correspondingly poor: $R(F) = 10.03\%$, $R_w(F) = 11.12\%$ (166 observed reflections with $I > 3\sigma(I)$). Attempted refinements in the other cubic space groups and lower-symmetry subgroups of $P\bar{4}3m$ did not lead to any improvement in the initial model.

When it became apparent from the X-ray powder data for $Na_3Zn_4O(PO_4)_3 \cdot 6H_2O$ that this structural model only represents a subcell of the true crystal structure, analysis of the single-crystal X-ray data was suspended, and efforts were made to model the structure by Rietveld refinements, using the 7.6 Å $P\bar{4}3m$ atomic parameters as a starting subcell model for the larger cells.

X-ray Rietveld Refinements. High-resolution X-ray powder data were collected for cubic $Rb_3Zn_4O(PO_4)_3 \cdot 3.5H_2O$ ($15° < 2\theta < 90°$), $Na_3Zn_4O(PO_4)_3 \cdot 6H_2O$ ($18° < 2\theta < 100°$), and $K_3Zn_4O(AsO_4)_3 \cdot 4H_2O$ ($15° < 2\theta < 100°$), on a Scintag PAD-X diffractometer (flat-plate sample; ~12-h scan; Cu Kα radiation: $\lambda = 1.541\,78$ Å; $\theta-\theta$ geometry; step size = 0.02°).

Possible starting atomic models for the Zn/X/O framework in space groups $F\bar{4}3c$ and $F\bar{4}3m$ were developed from the $P\bar{4}3m$ subcell framework atomic coordinates as derived from the single-crystal study of $Na_3Zn_4O(PO_4)_3 \cdot 6H_2O$. These two space groups represent the "well-behaved" cell-doubling symmetry transformations from a primitive cubic to a face-centered cubic unit cell. The atomic model in $F\bar{4}3c$ required four atomic species (1 Zn, 1 P, 2 O) to fully describe the Zn/P/O framework, while that in $F\bar{4}3m$ required six atoms (2 Zn, 1 P, 3 O). The $F\bar{4}3c$ model was used in the initial refinements for both $Rb_3Zn_4O(PO_4)_3 \cdot 3.5H_2O$ and $Na_3Zn_4O(PO_4)_3 \cdot 6H_2O$ and proved satisfactory. Attempting to model the $Rb_3Zn_4O(PO_4)_3 \cdot 3.5H_2O$ data in space group $F\bar{4}3m$ resulted in unstable refinements and very high correlations between related atomic and thermal parameters, and this model was discarded.

The Rietveld refinements (program: GSAS[19]) optimizing the framework-atom configurations in $Rb_3Zn_4O(PO_4)_3 \cdot 3.5H_2O$, $Na_3Zn_4O(PO_4)_3 \cdot 6H_2O$, and $K_3Zn_4O(AsO_4)_3 \cdot 4H_2O$ progressed normally and profile and atomic parameters were added to the model as variables in the normal way. A pseudo-Voigt function was used to describe the X-ray line shape, and a refinable Fourier cosine series described the background function. As the refinements converged, the nonframework species were located from Fourier difference maps and added to the refinement as additional atomic species.

For $Rb_3Zn_4O(PO_4)_3 \cdot 3.5H_2O$, the largest difference-map maximum was located at ($^1/_4$, $^1/_4$, ~±0.05), slightly offset from the center of the 8-ring window, and was assigned to Rb^+, resulting in a substantial improvement in fit. A close Rb(1)···Rb(1) contact prevents greater than 50% occupation of this site, and the Rb(1) site occupancy was initially set to 0.50. Further refinement cycles and repeated Fourier maps revealed a well-defined site in the cage region. Assigning this site to a water molecule (oxygen atom) and refining its positional and thermal parameters led to a negative U_{iso} value for this atom. A model was tried which assigned joint oxygen/rubidium character to this site and refined to give fractional occupancies of ~88:12

(15) Phillips, M. L. F.; Harrison, W. T. A.; Stucky, G. D.; McCarron III, E. M.; Calabrese, J. C.; Gier, T. E. *Chem. Mater.* **1992**, *4*, 222.

(16) Lehmann, M. S.; Larsen, F. K. *Acta Crystallogr.* **1974**, *A30*, 580.

(17) Sheldrick, G. M. SHELXS-86 User Guide, Crystallography Department, University of Göttingen, Germany, 1985.

(18) Watkin, D. J.; Carruthers, J. R.; Betteridge, P. W. CRYSTALS User Guide, Chemical Crystallography Laboratory, Oxford University, UK, 1990.

(19) Larson, A. C.; Von Dreele, R. R. GSAS User Guide, Los Alamos National Laboratory, Los Alamos, NM, 1992.

Table 1. Crystallographic Parameters

	$Rb_3Zn_4O(PO_4)_3 \cdot 3.5H_2O$	$K_3Zn_4O(AsO_4)_3 \cdot 4H_2O$	$Na_3Zn_4O(PO_4)_3 \cdot 6H_2O$
emp formula	$Rb_3Zn_4P_3O_{17}H_8$	$K_3Zn_4As_3O_{17}H_8$	$Na_3Zn_4P_3O_{19}H_{12}$
formula wt	881.40	883.63	739.49
crystal system	cubic	cubic	rhombohedral
habit	white powder	white powder	clear cuboid
$a = b = c$ (Å)	15.3423(9)	15.4638(2)	10.7489(3)
$\alpha = \beta = \gamma$ (deg)	90	90	60.114(2)
V (Å^3)	3611.4(6)	3697.9(2)	880.4(4)
Z	8	8	2
space group	$F\bar{4}3c$ (No. 219)	$F\bar{4}3c$ (No. 219)	$R3c$ (No. 161)
T (°C)	25(2)	25(2)	25(2)
λ (Å)	1.54178	1.54178	0.71073
ϱ_{calc} (g/cm^3)	3.27	3.17	2.79
no. of data	1874[a]	2124[a]	846[b]
no. of params	27	24	180
R_p[c] (%)	5.12	8.69	2.49[d]
R_{wp}[e] (%)	6.78	11.42	2.61[f]

[a] Number of data points. [b] Observed reflections with $I > 3\sigma(I)$ (single-crystal data). [c] $R_p = 100\sum|y_o - \mathbf{C}y_c|/\sum|y_o|$. [d] $R = 100\sum||F_o| - |F_c||/\sum|F_o|$. [e] $R_{wp} = 100[\sum w(y_o - \mathbf{C}y_c)^2/\sum wy_o^2]^{1/2}$, where $\mathbf{C}$ is a scale factor and $w_i = 1/\sigma_i^2$. [f] $R_w = 100[\sum w(|F_o| - |F_c|)^2/\sum w|F_o|^2]^{1/2}$.

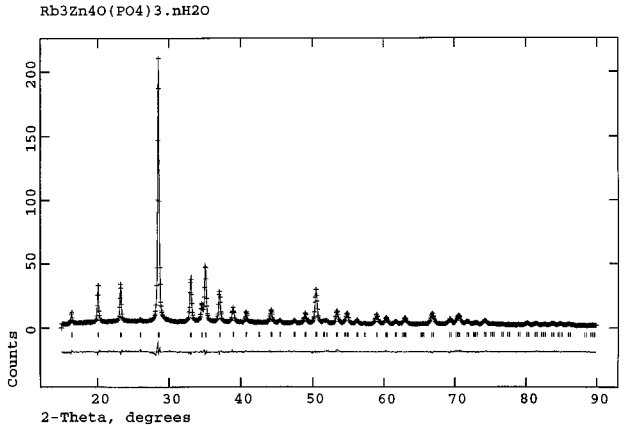

Figure 1. Final observed (crosses), calculated (line), and difference profiles for the X-ray Rietveld refinement for $Rb_3Zn_4O(PO_4)_3 \cdot 3.5H_2O$. Allowed reflection positions are indicated by tick marks.

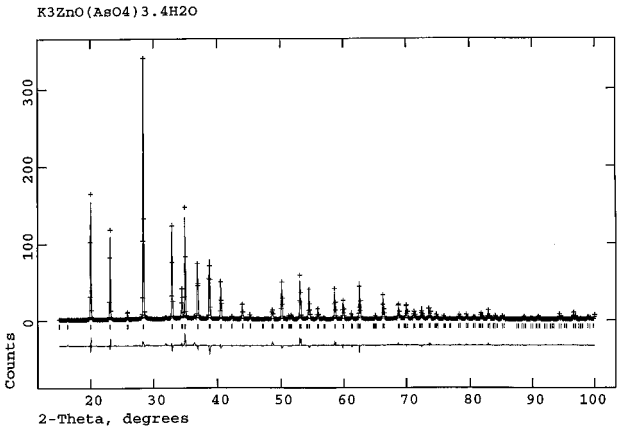

Figure 2. Final observed (crosses), calculated (line) and difference profiles for the X-ray Rietveld refinement for $Rb_3Zn_4O(PO_4)_3 \cdot 3.5H_2O$. Allowed reflection positions are indicated by tick marks.

O:Rb and a reasonable thermal parameter. Further sites were also apparent in the 8-ring window region, including a peak at ($^1/_4$, $^1/_4$, 0), in the center of the channel. Various models involving multiple, partially occupied, Rb atom sites in the 8-ring window region were tried and led to slight improvement in profile fit, but their physical significance is not clear. The final least-squares cycles simply modeled Rb(1) at ($^1/_4$, $^1/_4$, $\pm x$) as anisotropic and resulted in significant "smearing" of this atom in the channel direction. At the same time, the occupancy of Rb(1) was successfully refined to a chemically reasonable value.

Convergence for the $Rb_3Zn_4O(PO_4)_3 \cdot 3.5H_2O$ refinement was achieved with disagreement value of $R_p = 5.12\%$, $R_{wp} = 6.78\%$, and $R_{F^2} = 7.21\%$ (Table 1). The final observed, calculated and difference Rietveld profile plots for $Rb_3Zn_4O(PO_4)_3 \cdot 3.5H_2O$ are illustrated in Figure 1.

The $K_3Zn_4O(AsO_4)_3 \cdot 4H_2O$ refinement proceeded in similar fashion to that for $Rb_3Zn_4O(PO_4)_3 \cdot 3.5H_2O$, in space group $F\bar{4}3c$. The starting framework model was that of $Rb_3Zn_4O(PO_4)_3 \cdot 3.5H_2O$, with As replacing P. After initial refinement cycles, the extraframework species were located from difference Fourier maps. As with the $Rb_3Zn_4O(PO_4)_3 \cdot 3.5H_2O$ refinement, several sites in the 8-ring window and a well-defined site in the cage were apparent. Various atomic models were tried, but the simplest of these to give an acceptable profile fit was finally chosen, involving a single K^+ species, offset from the 8-ring channel center ($^1/_4$, $^1/_4$, 0), and a water molecule (O atom) in the spherical cage. This model is essentially the same as that for the extraframework species in $Rb_3Zn_4O(PO_4)_3 \cdot 3.5H_2O$. Further cycles of least-squares refinement led to convergence with disagreement values of $R_p = 8.69\%$, $R_{wp} = 11.42\%$, and $R_{F^2} = 11.05\%$. The final observed, calculated, and difference Rietveld profile plots for $K_3Zn_4O(AsO_4)_3 \cdot 4H_2O$ are illustrated in Figure 2.

For $Na_3Zn_4O(PO_4)_3 \cdot 6H_2O$, the $F\bar{4}3c$ model refinement converged to give a satisfactory profile fit ($R_p \approx 10\%$) after extraframework species were located from difference maps and included in the model, but close examination of the powder profile revealed the presence of several weak peaks forbidden in space group $F\bar{4}3c$ (absence conditions: $0kl$, k, $1 \neq 2n$; hhl, h, $l \neq 2n$; $00l$, $l \neq 2n$). Lowering the symmetry to $F23$ (absence conditions: $0kl$, k, $l \neq 2n$; hhl, $h + l \neq 2n$; $00l$, $l \neq 2n$) allowed for all the peaks to be indexed on the 15.2 Å face-centered cell. Revised atomic parameters were generated for the $F23$ model, and the refinement procedure was repeated. Several extraframework species were located from Fourier maps. After further damped refinement cycles, to ensure optimal convergence of the atomic positional and thermal parameters (occupational parameters also optimized for the nonframework species), the least-squares refinement converged to give acceptable final disagreement indexes of $R_p = 7.64\%$, $R_{wp} = 10.85\%$, and $R_{F^2} = 11.52\%$. Despite an excellent profile fit (Figure 3), the geometrical parameters derived from the best-fit solution indicated an unrealistically high degree of distortion of the ZnO_4, and especially the PO_4 framework species, and large uncertainties in the positions, thermal factors, and occupancies of the extraframework atoms. At this stage of our investigation, we attributed these problems to pseudosymmetry of the $F23$ model with respect to the $F\bar{4}3c$ model.

Second Single-Crystal Study of $Na_3Zn_4O(PO_4)_3 \cdot 6H_2O$. Because the X-ray Rietveld refinement for $Na_3Zn_4O(PO_4)_3 \cdot 6H_2O$ in space group $F23$ resulted only in fair geometrical parameters for the framework atoms and significant ambiguity with respect to the identities of extraframework species, a second single-crystal study on $Na_3Zn_4O(PO_4)_3 \cdot 6H_2O$ was carried out in an attempt to resolve these structural questions.

A clear, cube-shaped crystal (0.17 × 0.17 × 0.17 mm) of $Na_3Zn_4O(PO_4)_3 \cdot 6H_2O$ was mounted on a thin glass fiber with 5-min

Table 2. Atomic Positional/Thermal Parameters for $Rb_3Zn_4O(PO_4)_3 \cdot 3.5H_2O$

atom	W^a	x	y	z	U_{iso} (Å^2)	occ^b
Rb(1)	48*g*	1/4	1/4	0.0564(5)	0.17(5)^c	0.405(9)
Zn(1)	32*e*	0.07369(9)	0.07369	0.07369	0.010(1)	
P(1)	24*d*	1/4	0	0	0.010(1)	
O(1)	9*a*	0	0	0	0.023(3)	
O(2)	96*h*	0.0298(5)	0.0779(6)	0.1926(5)	0.023(3)	
O(3)^d	32*e*	−0.1634(3)	−0.1634	−0.1634	0.069(6)	

^{a} Wyckoff letter. ^{b} Fractional site occupancy, if not unity. ^{c} U_{eq}. ^{d} O(3) site occupied by 0.881(8) O (water molecule) and 0.119 Rb.

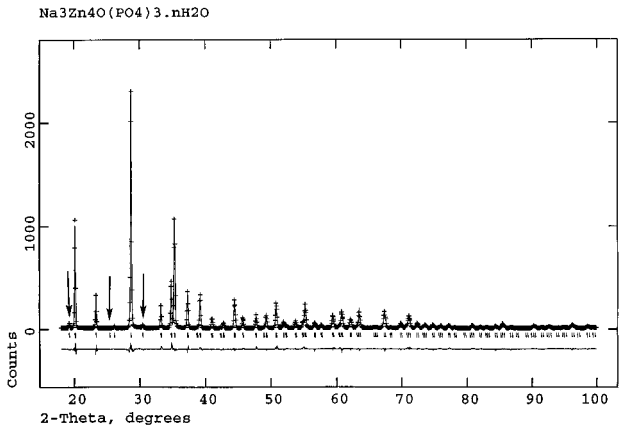

Figure 3. Final observed (crosses), calculated (line), and difference profiles for the pseudo solution in space group *F*23 for the X-ray Rietveld refinement for $Rb_3Zn_4O(PO_4)_3 \cdot 3.5H_2O$. Allowed reflection positions are indicated by tick marks. The low-angle reflections forbidden in space group $F\bar{4}3c$ are indicated by arrows.

epoxy glue. The unit-cell dimensions were determined from a least-squares refinement of the setting angles of 26 reflections ($30° < 2\theta < 40°$) and resulted in a face-centered cubic cell ($a \approx 15.2$ Å), based on reduction to the highest possible symmetry unit cell. A full sphere of intensity data ($0° < 2\theta < 60°$) was collected as described above for the initial study of $Na_3Zn_4O(PO_4)_3 \cdot 6H_2O$ (Huber automated diffractometer, Mo Kα radiation, $\lambda = 0.710\ 73$ Å). An empirical absorption correction using ψ-scan data was applied (equivalent transmission factors range: 0.414−0.523).

On data merging, problems were apparent in cubic symmetry. A poor merging *R* factor of ∼14% resulted, and visual inspection of the reduced data revealed many gross discrepancies between reflections with supposedly equivalent intensities. The only reasonable merging scheme was one that assumed triclinic symmetry for this material (i.e., only Friedel pairs merged). An attempt to model the 15.2 Å FCC single crystal data with the *F*23 Rietveld refinement atomic model for $Na_3Zn_4O(PO_4)_3 \cdot 6H_2O$ led to a poor fit and problems with the model similar to those experienced in the X-ray Rietveld refinement for the same phase. Various models supposing twinning were tried but did not lead to improvements in fit.

The same crystal of $Na_3Zn_4O(PO_4)_3 \cdot 6H_2O$ was mounted on a Siemens Smart-CCD diffractometer (position-sensitive detector) equipped with a normal focus, 3 kW sealed tube X-ray source (Mo Kα radiation, $\lambda = 0.710\ 73$ Å). At −150 °C, a least-squares fit to centered, high-angle reflections revealed a hexagonal unit cell (*R* centered) with $a = 10.7305(6)$ Å and $c = 26.2190(3)$ Å ($V = 2614.5$ Å^3). The primitive rhombohedral setting of this cell ($a = 10.713$ Å, $\alpha = 60.11°$, $V = 871.5$ Å^3) is pseudo-face-centered cubic ($a = 15.162$ Å, $\alpha = 90.09°$).

After the low-temperature study revealed a rhombohedral/hexagonal cell, the pseudo-FCC room-temperature data were examined once again. Careful examination of the pseudo-cubic *hhh* type reflections revealed systematic anomalies: Two out of eight of each of the *hhh*-type reflection groups [(−*h*, −*h*, +*h*) and its Friedel equivalent] were clearly different in intensity from the other six reflections, which showed acceptable consistency among themselves. The FCC data were thus transformed twice; first, to translate these two reflections to the (−*h*, −*h*, −*h*) and (+*h*, +*h*, +*h*) indexes corresponding to the ⟨111⟩ body diagonal of the face-centered-cubic cell, and second to reduce the overall symmetry to primitive rhombohedral,[20] such that $a_r \approx (\sqrt{2}/2)a_c$ and $\alpha \approx 60°$ for the transformed cell. The systematic absence conditions in the transformed data (*hhl*, $l \neq 2n$; *hhh*, $h \neq 2n$) corresponded to space groups *R*3*c* (No. 161) or $R\bar{3}c$ (No. 167).

Table 3. Selected Bond Distances (Å)/Angles (deg) for $Rb_3Zn_4O(PO_4)_3 \cdot 3.5H_2O$

Zn(1)−O(1)	1.958(3)	Zn(1)−O(2) × 3	1.945(6)
P(1)−O(2) × 4	1.553(8)		
Rb(1)−O(2) × 2	2.81(1)	Rb(1)−O(2) × 2	3.082(8)
Rb(1)−O(3) × 2	2.495(6)		
O(1)−Zn(1)−O(2) × 3	111.2(4)	O(2)−Zn(1)−O(2) × 3	107.8(4)
O(2)−P(1)−O(2) × 2	110.9(7)	O(2)−P(1)−O(2) × 4	108.8(4)
Zn(1)−O(1)−Zn(1) × 6	109.47^a	Zn(1)−O(2)−P(1)	127.5(5)

^{a} By symmetry.

After these transformations to rhombohedral symmetry, a very satisfactory data merging was accomplished [10 494 reflections entered; $R_{Int} = 4.38\%$; 846 observed reflections with $I > 3\sigma(I)$ after merging]. The initial structural model was established in space group *R*3*c* by direct methods by SHELXS-86,[17] and the refinement was carried out using CRYSTALS.[18] This rapidly converged, and the remaining atoms were easily found by difference Fourier syntheses and added to the model. No starting model could be established in space group $R\bar{3}c$, and the noncentrosymmetric space group was assumed for the remainder of the data analysis. This is consistent with the nonzero PSHG signal observed for $Na_3Zn_4O(PO_4)_3 \cdot 6H_2O$. We note that *R*3*c* represents a "well-behaved" symmetry-lowering transformation from $F\bar{4}3c$ as found for the face-centered cubic structures in this family of phases.

The *R*3*c* atomic model was tried against the X-ray powder data and refined well. This powder refinement allowed for more accurate rhombohedral cell parameters to be obtained, and these values were subsequently used in the single-crystal study (Table 1).

The *R*3*c* single-crystal model refined to convergence straightforwardly to final residuals of $R = 2.49\%$ and $R_w = 2.61\%$, as summarized in Table 1. An extinction correction was optimized in the latter refinement cycles, and the final difference map (min = −0.42, max = +0.56 e/Å) was essentially featureless. Refinement of the *R*3*c* $Na_3Zn_4O(PO_4)_3 \cdot 6H_2O$ atomic model against the −150 °C data resulted in a solution essentially identical with the room-temperature result. Anisotropic thermal factors and final observed and calculated structure factors for $Na_3Zn_4O(PO_4)_3 \cdot 6H_2O$ are available as supporting information.

Results

$Rb_3Zn_4O(PO_4)_3 \cdot 3.5H_2O$. Final atomic positional and thermal parameters for $Rb_3Zn_4O(PO_4)_3 \cdot 3.5H_2O$ are presented in Table 2, with selected bond distance/angle data in Table 3. $Rb_3Zn_4O(PO_4)_3 \cdot 3.5H_2O$ consists of a new type of three-dimensional, microporous zincophosphate framework, enclosing guest rubidium cations and water molecules. One zinc atom (tetrahedral), one phosphorus atom (tetrahedral), and two oxygen atoms make up the framework asymmetric unit of the structure (Figure 4). Bond distances and angles for these species are in good agreement with previous structure

(20) *International Tables for X-Ray Crystallography*; Kluwer Academic Press: Dordrecht, 1992; Vol. A, Table 5.1.

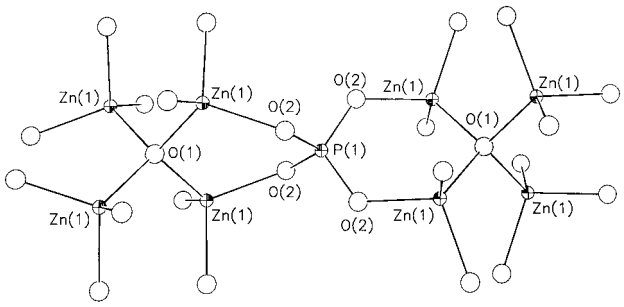

Figure 4. Detail of the $Rb_3Zn_4O(PO_4)_3 \cdot 3.5H_2O$ structure, showing the framework-atom connectivity. Note the tetrahedrally coordinated O(1) oxygen species (arbitrary atom radii). All the unlabeled atoms are O(2) species. This ZnO_4/PO_4 connectivity results in tetrahedral 3-rings joined into a spiro-5 configuration (see text).

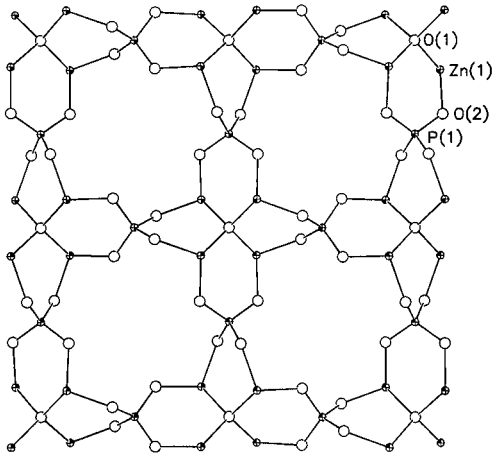

Figure 5. [001] projection of a layer ($-0.15 < z < 0.15$) of the $Rb_3Zn_4O(PO_4)_3 \cdot 3.5H_2O$ structure, showing the connectivity of four spiro-5 units into 8-ring windows.

determinations of Zn/P/O tetrahedral framework materials.[4,8] Zn(1) (site symmetry .3.) bonds to O(1) and 3 × O(2) in regular tetrahedral geometry (d_{av}[Zn−O] = 1.948(5) Å), and P(1) (site symmetry 4..) makes four equivalent bonds to O(2). One oxygen atom, O(1), located at (0, 0, 0) and its equivalent positions (site symmetry 23.) is surrounded by a tetrahedron of *four* zinc atoms, and the other oxygen atom, O(2) (general position), forms a more typical bicoordinate Zn−O−P bridge. This results in a framework configuration of $[Zn_4O(PO_4)_3]^{3-}$ (Figures 5 and 6), which is charge balanced by the guest Rb^+ cations.

The most interesting structural feature of the $Rb_3Zn_4O(PO_4)_3 \cdot 3.5H_2O$ framework is the presence of tetrahedral OZn_4 clusters at the corners, edges, and face centers of the unit cell. These clusters are linked via phosphate groups into the Zn/P/O framework configuration, which results in large, roughly spherical cavities, interlinked by a three-dimensional network of tilted 8-ring channels, propagating in the orthogonal [100], [010], and [001] directions (Figure 7). Unusual tetrahedral 3-rings, built up from 2 × ZnO_4 and 1 × PO_4, linked via Zn−O−Zn′ and Zn−O−P bonds, are present in the framework (Figure 6). These 3-rings are paired into spiro-5-type subunits, which have only been previously seen in the novel beryllosilicate phase lovdarite.[21] One [001] "layer" of tilted 8-rings is illustrated in Figure 5. In the 7.6 Å $P\bar{4}3m$ subcell model, these 8-rings are regular in shape (i.e., they are untilted).

(21) Merlino, S. *Eur. J. Mineral.* **1990**, *2*, 809.

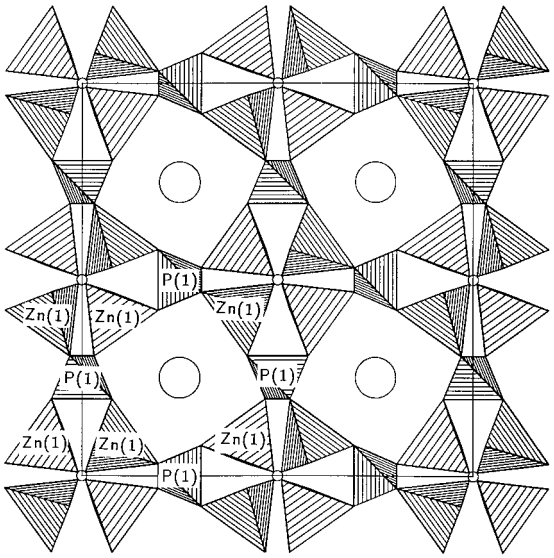

Figure 6. [001] polyhedral projection of the $Rb_3Zn_4O(PO_4)_3 \cdot 3.5H_2O$ structure, showing the spiro-5 framework building units and tilted 8-ring intercage windows occupied by rubidium cations. The tetrahedral O(1) species are indicated by small circles.

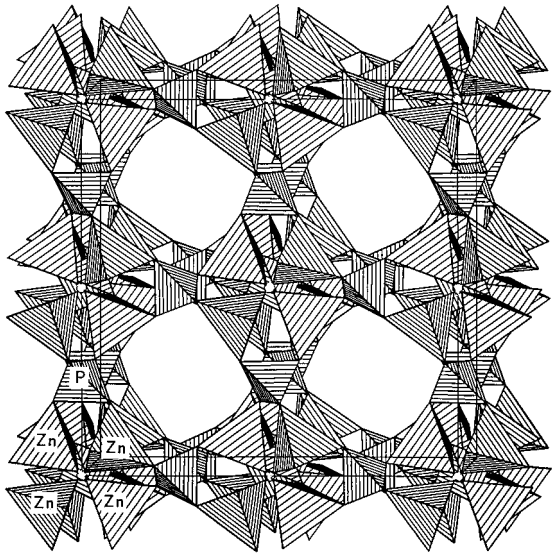

Figure 7. Polyhedral plot of the framework of $Rb_3Zn_4O(PO_4)_3 \cdot 3.5H_2O$, viewed just oblique to [001], showing the spherical cavities, and intercavity 8-ring channels.

The X-ray profile refinement indicated that the extraframework species are highly mobile in $Rb_3Zn_4O(PO_4)_3 \cdot 3.5H_2O$, which is typical of zeolite-like systems. The Rb(1) species occupies a ($^1/_4$, $^1/_4$, $\pm z$) position (site symmetry ..2), slightly displaced from the center ($^1/_4$, $^1/_4$, 0) of each 8-ring channel and makes four Rb−O(2) bonds to the framework, in 2 + 2 configuration (Table 3, Figure 8). If the Rb^+ species occupied the channel center, then four equivalent Rb−O(2) bonds would result. Each Rb^+ species also bonds to two extraframework water molecules (oxygen atoms), located in the same cage. The water molecule [O(3)] bonds to three Rb(1) species in roughly triangular geometry. There are four of these O(3) atoms in each cage. The refined unit-cell composition, based on the Rietveld refinement, is $Rb_{2.88}Zn_4O(PO_4)_3 \cdot 3.5H_2O$, in fairly good agreement with the requirement for 3.00 Rb^+ species for charge-balancing purposes and in excellent agreement with the 3.5 H_2O per formula unit from the TGA results.

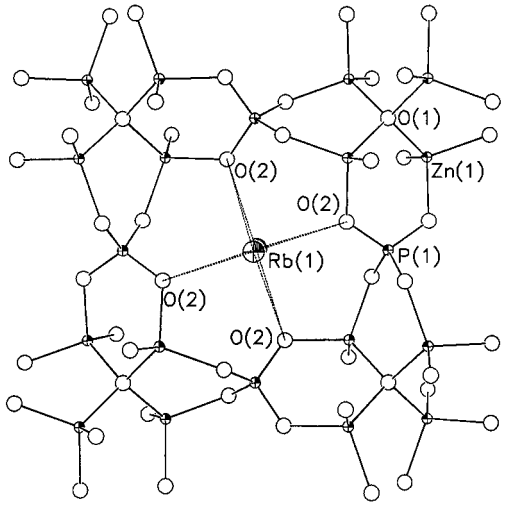

Figure 8. Detail of one 8-ring window in $Rb_3Zn_4O(PO_4)_3 \cdot 3.5H_2O$, showing the four Rb(1) to framework oxygen atom bonds.

Table 4. Atomic Positional Parameters for $K_3Zn_4O(AsO_4)_3 \cdot 4H_2O$

atom	W^a	x	y	z	U_{iso} (Å^2)	occ^b
K(1)	48*g*	1/4	1/4	0.0595(6)	0.162(5)	1/2
Zn(1)	32*e*	0.07333(8)	0.07333	0.07333	0.0146(8)	
As(1)	24*d*	1/4	0	0	0.0169(8)	
O(1)	8*a*	0	0	0	0.008(2)	
O(2)	96*h*	0.0219(5)	0.0876(5)	0.1887(4)	0.008(2)	
O(3)^c	32*e*	−0.1683(5)	−0.1683	−0.1683	0.130(6)	

^{a} Wyckoff letter. ^{b} Fractional site occupancy, if not unity. ^{c} Water molecule oxygen atom.

Table 5. Selected Bond Distances (Å)/Angles (deg) for $K_3Zn_4O(AsO_4)_3 \cdot 4H_2O$

Zn(1)−O(1)	1.964(3)	Zn(1)−O(2) × 3	1.966(3)
As(1)−O(2) × 4	1.687(7)		
K(1)−O(2) × 2	2.747(8)	K(1)−O(2) × 2	2.965(7)
K(1)−O(3) × 2	2.455(7)		
O(1)−Zn(1)−O(2) × 3	110.8(3)	O(2)−Zn(1)−O(2) × 3	108.1(3)
O(2)−As(1)−O(2) × 2	111.7(5)	O(2)−As(1)−O(2) × 4	108.4(3)
Zn(1)−O(1)−Zn(1) × 6	109.47^a	Zn(1)−O(2)−As(1)	120.1(4)

^{a} By symmetry.

$K_3Zn_4O(AsO_4)_3 \cdot 4H_2O$. Refined atomic positional and thermal parameters for $K_3Zn_4O(AsO_4)_3 \cdot 4H_2O$ are presented in Table 4, with selected geometrical data given in Table 5. $K_3Zn_4O(AsO_4)_3 \cdot 4H_2O$ crystallizes in the same space group ($F\bar{4}3c$) as $Rb_3Zn_4O(PO_4)_3 \cdot 3.5H_2O$, with As substituting for P in the framework and K replacing Rb as an extraframework species. Bond distances and angles for the framework species in $K_3Zn_4O(AsO_4)_3 \cdot 4H_2O$ are in good agreement with previous structure determinations of Zn/As/O tetrahedral framework materials,[6] and the As−O bond shows its expected length of 1.687(7) Å. The Zn(1)−O(2)−As(1) bond angle (in the 8-ring) in $K_3Zn_4O(AsO_4)_3 \cdot 4H_2O$ is 120.1(4)°, compared with 127.5(5)° for the equivalent Zn−O−P bond angle in $Rb_3Zn_4O(PO_4)_3 \cdot 3.5H_2O$. A similar trend in bond-angle reduction in moving from phosphate to arsenate has also been observed in sodalite-type phases,[22] although here, the different guest cations (K and Rb) may also play a structural role in defining exact framework geometry.

The two well-defined guest sites in $K_3Zn_4O(AsO_4)_3 \cdot 4H_2O$ were modeled as one potassium cation and one water molecule, which led to a stable refinement and resulted in reasonable geometrical parameters for the guest species. The potassium cation, K(1), with a site occupation factor of 0.5, occupies a site near the center of the inter-cage window at (1/4, 1/4, ±0.0595(6)), and makes four bonds with nearby framework O(2) atoms (compare Figure 8), and two bonds to water molecules [O(3) atoms] in the same cage into which the disordered K^+ cation projects (by 0.92 Å from the intercage channel midpoint). The water molecule [O(3)] bonds to three distinct K(1) species in almost triangular geometry: a rather similar bonding geometry was observed for the water molecule in the pharmacosiderite-type $Cs_3HTi_4O_4(SiO_4)_3 \cdot 4H_2O$, in which each H_2O species makes three O···Cs contacts to Cs^+ species occupying disordered sites near the 8-ring windows.[12] The H-bonding configuration (if any) of the water molecule is unknown in $K_3Zn_4O(AsO_4)_3 \cdot 4H_2O$: several O(3)···$O_f$ contacts of 2.8−3.0 Å are present. $K_3Zn_4O(AsO_4)_3 \cdot 4H_2O$ is essentially isostructural with $Rb_3Zn_4O(PO_4)_3 \cdot 3.5H_2O$ in terms of both framework and nonframework species.

Table 6. Atomic Positional/Thermal Parameters for $Na_3Zn_4O(PO_4)_3 \cdot 6H_2O$

atom	x	y	z	U_{eq}^{a}
Na(1)	−0.0999(5)	−0.4905(4)	0.6232(4)	0.0513
Zn(1)	0.08329(7)	−0.22412(7)	0.06804(7)	0.0158
Zn(2)^b	0.07237(5)	0.07237	0.07237	0.0161
P(1)	−0.2321(2)	−0.2655(2)	0.2642(2)	0.0159
O(1)^b	−0.0002(2)	−0.0002	−0.0002	0.0149
O(2)	−0.0699(5)	−0.3150(5)	0.1536(5)	0.0232
O(3)	0.1551(5)	−0.2826(5)	0.2317(5)	0.0250
O(4)	0.2578(4)	−0.2753(5)	−0.1042(5)	0.0233
O(5)	0.2574(5)	−0.0709(5)	0.1258(5)	0.0240
O(6)^c	0.5218(6)	−0.1210(6)	0.7681(6)	0.0414
O(7)^c	0.6269(6)	−0.0799(6)	−0.0680(6)	0.0473

^{a} U_{eq} (Å^2) = $(U_1U_2U_3)^{1/3}$. ^{b} Wyckoff site 2a. ^{c} Water molecule oxygen atom.

Table 7. Selected Bond Distances (Å) and Angles (deg) for $Na_3Zn_4O(PO_4)_3 \cdot 6H_2O$

Na(1)−O(2)	2.886(6)	Na(1)−O(4)	2.376(5)
Na(1)−O(5)	2.636(6)	Na(1)−O(5)	2.929(6)
Na(1)−O(6)	2.425(6)	Na(1)−O(6)	2.359(6)
Na(1)−O(7)	2.427(7)		
Zn(1)−O(1)	1.970(2)	Zn(1)−O(2)	1.926(4)
Zn(1)−O(3)	1.963(4)	Zn(1)−O(4)	1.943(4)
Zn(2)−O(1)	1.909(6)	Zn(2)−O(5) × 3	1.965(4)
P(1)−O(2)	1.542(4)	P(1)−O(3)	1.544(4)
P(1)−O(4)	1.529(4)	P(1)−O(5)	1.545(4)
O(1)−Zn(1)−O(2)	112.2(2)	O(1)−Zn(1)−O(3)	105.3(2)
O(2)−Zn(1)−O(3)	107.4(2)	O(1)−Zn(1)−O(4)	105.6(1)
O(2)−Zn(1)−O(4)	116.8(2)	O(3)−Zn(1)−O(4)	108.9(2)
O(1)−Zn(2)−O(5) × 3	115.1(1)	O(5)−Zn(2)−O(5) × 3	103.3(2)
O(2)−P(1)−O(3)	109.0(3)	O(2)−P(1)−O(4)	110.2(2)
O(3)−P(1)−O(4)	109.0(2)	O(2)−P(1)−O(5)	110.6(3)
O(3)−P(1)−O(5)	109.3(2)	O(4)−P(1)−O(5)	108.7(3)
Zn(1)−O(1)−Zn(1) × 3	110.2(2)	Zn(1)−O(1)−Zn(2) × 3	108.7(2)
Zn(1)−O(2)−P(1)	126.1(3)	Zn(1)−O(3)−P(1)	131.1(3)
Zn(1)−O(4)−P(1)	128.8(3)	Zn(2)−O(5)−P(1)	121.1(3)

$Na_3Zn_4O(PO_4)_3 \cdot 6H_2O$. The final atomic positional and thermal parameters (Table 6) and selected bond distance/angle parameters (Table 7) for $Na_3Zn_4O(PO_4)_3 \cdot 6H_2O$ indicate a similar overall structure to those of $Rb_3Zn_4O(PO_4)_3 \cdot 3.5H_2O$ and $K_3Zn_4O(AsO_4)_3 \cdot 4H_2O$, although the symmetry has been lowered to rhombohedral (space group $R3c$) for the sodium-containing phase. The $[Zn_4O(PO_4)_3]^{3-}$ framework topology is unchanged, compared to that of $Rb_3Zn_4O(PO_4)_3 \cdot 3.5H_2O$, although in rhombohedral symmetry there are now eight crystallographically distinct framework atoms (2 × Zn, 1 × P, 5 × O). All these atoms occupy general

(22) Nenoff, T. M.; Harrison, W. T. A.; Gier, T. E.; Keder, N. L.; Zaremba, C. M.; Srdanov, V. I.; Nicol, J. M.; Stucky, G. D. *Inorg. Chem.* **1994**, *3*, 2472.

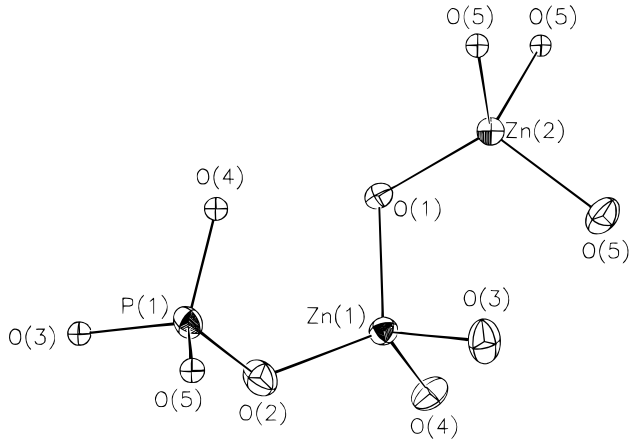

Figure 9. Detail of the $Na_3Zn_4O(PO_4)_3 \cdot 6H_2O$ framework, showing connectivity and labeling scheme.

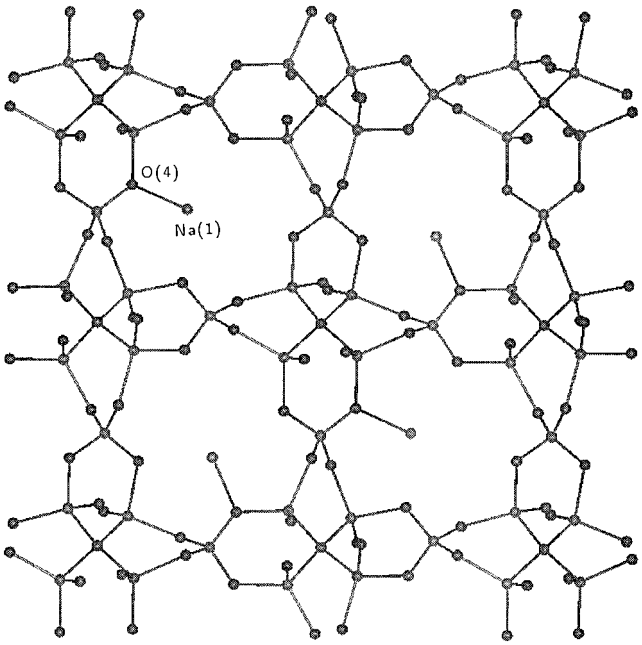

Figure 10. [011] projection of the rhombohedral $Na_3Zn_4O(PO_4)_3 \cdot 6H_2O$ structure, showing its relationship to the cubic $Rb_3Zn_4O(PO_4)_3 \cdot 3.5H_2O$ structure (compare Figure 5). The short Na(1)−O(4) bonds arising from the displacement of the sodium cations from the centers of the 8-ring windows are shown (see text). Note that the Na^+ species are ordered.

positions (Figure 9), except Zn(2) and O(1) (both (*x*, *x*, *x*) sites with 3. site symmetry). The bond distances and angles for the framework species; d_{av}(Zn−O) = 1.951(2) Å, d_{av}(P−O) = 1.540(2) Å; are in very good agreement with other crystallographic studies on Zn/P/O framework phases,[8,9] and the apparent angular and bond-length distortions of the PO_4 group observed in the *F*23 powder study are not apparent. The $Na_3Zn_4O(PO_4)_3 \cdot 6H_2O$ structure contains similar, slightly tilted, 8-ring intercavity channels (Figure 10) to those found in the $Rb_3Zn_4O(PO_4)_3 \cdot 3.5H_2O$ phase. Including extraframework atoms, the calculated density of $Na_3Zn_4O(PO_4)_3 \cdot 6H_2O$ is 2.79 g/cm^3. If the extraframework species (Na, H_2O) are neglected, the density of the $Na_3Zn_4O(PO_4)_3 \cdot 6H_2O$ framework is 2.06 g/cm^3 and a FD value[23] (number of *T* atoms/1000 Å^3) of 15.9 results. This FD value is comparable to those for the aluminosilicate zeolite erionite (International Zeolite Association code: ERI) and beryllophosphate-H (BPH).[24]

(23) Brunner, G. O.; Meier, W. M. *Nature (London)* **1989**, *337*, 146.

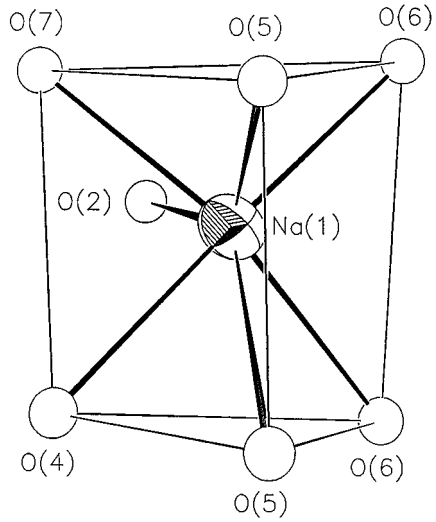

Figure 11. Detail showing the 7-fold sodium ion coordination in $Na_3Zn_4O(PO_4)_3 \cdot 6H_2O$.

The extraframework atoms in $Na_3Zn_4O(PO_4)_3 \cdot 6H_2O$ show significant differences as compared with the equivalent species in the $Rb_3Zn_4O(PO_4)_3 \cdot 3.5H_2O$ and $K_3Zn_4O(AsO_4)_3 \cdot 4H_2O$ structures. In $Na_3Zn_4O(PO_4)_3 \cdot 6H_2O$, the single-crystal data clearly revealed a single, fully occupied sodium site displaced toward the channel side from the center of the 8-ring window region, compared to the partially occupied, disordered, extraframework sites (occupying the central axis of the channel) assigned to Rb^+ in the rubidium phase. There are two distinct water molecules (oxygen atoms) in the cage region in $Na_3Zn_4O(PO_4)_3 \cdot 6H_2O$, as compared to just one cage site in $Rb_3Zn_4O(PO_4)_3 \cdot 3.5H_2O$ and $K_3Zn_4O(AsO_4)_3 \cdot 4H_2O$. In $Na_3Zn_4O(PO_4)_3 \cdot 6H_2O$, both these sites are fully occupied within experimental error, based on refinements of the site-occupancy factors of these atoms (assuming oxygen character only), resulting in a stoichiometry of six water molecules per framework formula unit. The 7-fold coordination polyhedron around the Na^+ species is approximately face-capped trigonal prismatic (Figure 11).

We may attribute the symmetry lowering of the $Na_3Zn_4O(PO_4)_3 \cdot 6H_2O$ structure from $F\bar{4}3c$ to $R3c$ to ordering of the guest sodium cations. Essentially, the Na^+ species moves away from the center of the eight-ring window toward the cage-wall to optimize its coordination with nearby O atoms (bond valence sum[25] for Na(1) = 1.00). As a result, in $Na_3Zn_4O(PO_4)_3 \cdot 6H_2O$, the sodium cation makes one short Na−O link to a framework oxygen atom [O(4)], three longer Na−O links to O(2) and 2 × O(5), and three Na−O bonds to water molecules (Table 7). The Zn(2)−O(5)−P(1) bond angle of 121.1(3)° is significantly smaller than the other Zn−O−P angles and also the equivalent Zn−O−P linkage in the rubidium congener. There is no obvious correlation between the Na^+ siting and the Zn(1)−O(4)−P(1) bond angle.

The establishment of the $Na_3Zn_4O(PO_4)_3 \cdot 6H_2O$ crystal structure described here illustrates some of the problems in determining molecular sieve structures by diffraction methods.[26] The initial single-crystal study

(24) FD values from: *Atlas of Zeolite Structure Types*; Meier, W. M., Olson, D. H., Eds.; Butterworth-Heinmann: London, 1992. Standard three-letter zeolite-type codes defined herein.

(25) Brese, N. E.; O'Keeffe, M. *Acta Crystallogr.* **1991**, *B47*, 192.

(26) McCusker, L. B. *Acta Crystallogr.* **1991**, *A47*, 297.

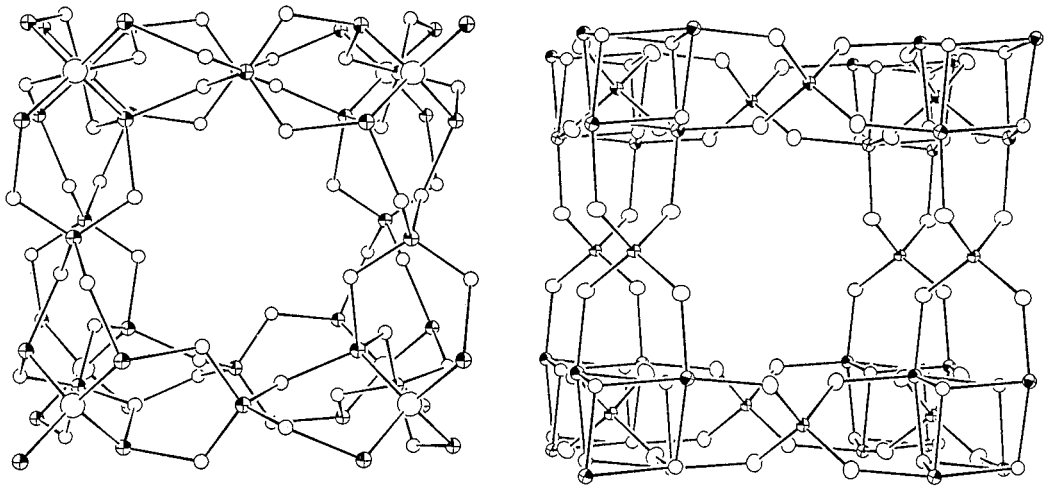

Figure 12. Views of the $M_3Zn_4O(XO_4)_3 \cdot nH_2O$ (left) and pharmacosiderite (right) frameworks, showing the relationship between these two structure types (see text for further details). For ease of comparison, one cage unit is shown for both structures, corresponding to approximate unit-cell limits of $-0.15 < x < 0.65$, $-0.15 < y < 0.65$, and $-0.15 < z < 0.65$ for the face centered cubic ($a \approx 15.2$ Å) $M_3Zn_4O(XO_4)_3 \cdot nH_2O$ structure, and $-0.1 < x < 1.1$, $-0.1 < y < 1.1$, and $-0.1 < z < 1.1$ for the primitive cubic ($a \approx 7.6$ Å) pharmacosiderite structure.

on $Na_3Zn_4O(PO_4)_3 \cdot 6H_2O$, which relied on black-box search and indexing routines only established a subcell of the true $Na_3Zn_4O(PO_4)_3 \cdot 6H_2O$ structure. After deduction of the supercell framework structure, powder methods were then apparently successful in determining the full $Na_3Zn_4O(PO_4)_3 \cdot 6H_2O$ structure, and a good profile fit was obtained (Figure 3). However, the refined atomic coordinates in space group *F*23 were not satisfactory. Only the low-temperature single-crystal cell determination revealed clear evidence of rhombohedral symmetry. Once this was clear, the single-crystal data could be transformed to *R*3*c* and successfully modeled. It is interesting to note that *F*23 and *R*3*c* are two of the well-behaved symmetry-reducing transformations from the $F\bar{4}3c$ prototype structure for this family of phases. We note that if a nominal sodium-ion displacement away from the channel center occurred in space group $F\bar{4}3c$, then a 4-fold disorder of sodium in the 8-ring window would result. If the same off-center displacement were to occur in the pseudosolution space group of *F*23 (X-ray Rietveld refinement for $Na_3Zn_4O(PO_4)_3 \cdot 6H_2O$), then a 2-fold disorder of Na^+ species would result. In *R*3*c*, there is no positional disorder of the Na^+ species. Thus, in $Na_3Zn_4O(PO_4)_3 \cdot 6H_2O$, the *guest cation* behavior is the key factor in determining the crystal symmetry.

Discussion

The $M_3Zn_4O(XO_4)_3 \cdot nH_2O$ phases reported here represent a large new family of zincophosphate/arsenate-based microporous materials, which show characteristic zeolitic behavior with respect to ion exchange and dehydration/rehydration. Pairs of 3-rings (nodal atoms: 2 × Zn, 1 × P/As, linked by Zn−O−Zn′ and Zn−O−P/As bonds) in spiro-5 configuration (nodal center: P) are the basic building block of the framework for these phases, and these link together to form 8-ring windows. This double-3-ring/8-ring framework topology is unique and has no obvious counterparts in other zincophosphate/arsenate materials or in aluminosilicates or other molecular sieve families.

These phases are also notable for the novel, tetrahedrally coordinated framework oxygen atom, through which *four* adjacent zinc atoms (as ZnO_4 tetrahedra) are joined. This type of tetrahedral oxygen connectivity is commonplace in condensed zinc-containing structures, including ZnO itself[27] but is without precedent in aluminosilicate or aluminophosphate molecular sieve structures. Some other open-framework and layered zincophosphate materials[9,28] contain *three*-coordinate oxygen atoms, which link to two adjacent Zn centers and one P neighbor, as opposed to the four Zn neighbors of the central O atom in these materials.

As observed in other three-dimensional tetrahedral zincophosphate materials, Zn−O−P and Zn−O−Zn bonds are favored, while P−O−P bonds are avoided. The presence of the tetrahedral OZn_4 group leads to "excess" zinc, and a 4:3 Zn:P ratio, which is emphasized if the framework formula unit is written as $[ZnO \cdot (ZnPO_4)_3]^{3-}$ (charge balancing in these phases by three univalent extraframework cations). Other three-dimensional, open-framework zincophosphates such as the sodalite-type $Na_3(ZnPO_4)_3 \cdot 4H_2O$[5] and ABW-type $NaZnPO_4 \cdot 4H_2O$[3] contain a Zn:P ratio of unity, akin to 1:1 Si:Al aluminosilicates. The faujasite-type $Na_{67}TMA_{12}Zn_8(ZnPO_4)_{96} \cdot 192H_2O$[4] (TMA = tetramethylammonium cation) contains both framework and extraframework zinc cations, and a 1:1 Zn:P *framework* ratio. These materials are built up from 4-rings and 6-rings of alternating, ordered ZnO_4 and PO_4 species. We are presently assessing if other divalent, or otherwise charged, tetrahedral cations can (partially) substitute for zinc in the $M_3Zn_4O(XO_4)_3 \cdot nH_2O$ structure.

The $M_3Zn_4O(XO_4)_3 \cdot nH_2O$ structure type is closely related to the octahedral/tetrahedral pharmacosiderite framework.[11,12] The pharmacosiderite structure (Figure 12) is based on a ~7.5 Å primitive cubic cell, although superstructures (unit-cell doublings)[29] and rhombohedral distortions[30] are also known, akin to those reported for the $M_3Zn_4O(XO_4)_3 \cdot nH_2O$ phases reported here. The 7.5 Å cube pharmacosiderite cell contains an octahedral/

(27) Schulz, H.; Thiemann, K. H. *Solid State Commun.* **1979**, *32*, 783.
(28) Nenoff, T. M.; Harrison, W. T. A.; Gier, T. E.; Calabrese, J. C.; Stucky, G. D. *J. Solid State Chem.* **1993**, *107*, 285.
(29) Mutter, G.; Eysel, W.; Greis, O.; Schmetzer, K. *N. Jb. Miner. Mh.* **1984**, *4*, 183.
(30) Nenoff, T. M.; Harrison, W. T. A.; Stucky, G. D. *Chem. Mater.* **1994**, *6*, 525.

Table 8. Summary of Sodium Zinc Phosphate Phases

formula	pH[a]	ratio[b]	structure	ref
$Zn_3(PO_4)_2 \cdot 4H_2O$	1−2	0:3:2	hopeite	33
$Na_2Zn(HPO_4)_2 \cdot 4H_2O$	2[c]	2:1:2	layered; 4- and 12-rings	34
$NaZn_2(PO_4)(HPO_4)$	2−4	1:2:2	corrugated layers; 3-, 4-rings	28
$Na_3(ZnPO_4)_3 \cdot 4H_2O$	6−8	1:1:1	sodalite; 4-, 6-rings	5
$Na_6Zn_3(PO_4)_4 \cdot 3H_2O$	10	6:3:4	semicondensed 3-dimensional	10
$NaZnPO_4 \cdot H_2O$	11	1:1:1	new chiral framework; 4-, 6-, 12-rings	13
$Na_3Zn_4O(PO_4)_3 \cdot 6H_2O$	12.5	3:4:3	novel 3-, 8-ring framework	this work
$Na_2Zn(OH)PO_4 \cdot 7H_2O$	13	2:1:1	novel 3-ring chain structure	35
ZnO	13+	0:1:0		27
$NaZn(OH)_3$	14[d]	2:1:0		36

[a] Starting solution pH. [b] Na:Zn:P molar ratio of solid product. [c] At 4 °C. [d] Concentrated NaOH solution.

tetrahedral framework, enclosing a three-dimensional channel/cavity system very like that found for the $M_3Zn_4O(XO_4)_3 \cdot nH_2O$ phases. In pharmacosiderite, a cluster of four octahedral MO_6 groups each share a face, resulting in a cubane-like M_4O_4 cluster at each unit-cell corner, which is equivalent to the tetrahedral OZn_4 corner units found in $M_3Zn_4O(XO_4)_3 \cdot nH_2O$ types. A difference between the two structure types is seen in the oxidation states of the framework cations: trivalent, tetravalent, and pentavalent octahedral species known to occur in the pharmacosiderite structure, whereas, so far, only divalent Zn is known in the $M_3Zn_4O(XO_4)_3 \cdot nH_2O$ type. "Mixed" phases containing a combination of M_4O_4 pharmacosiderite-type cubes and $M_3Zn_4O(XO_4)_3 \cdot nH_2O$-type OZn_4 tetrahedra represent an interesting synthetic challenge, which we are presently investigating.

The $M_3Zn_4O(XO_4)_3 \cdot nH_2O$ framework is quite flexible, as evidenced by the unit-cell distortions on ion-exchange noted in the Experimental Section, and this flexibility may well be significant in relation to the very high thermal stabilities of some of these materials. It seems likely that the framework distorts in order to optimize the coordination of the guest cation in the 8-ring window region. This degree of framework flexibility is less common in aluminosilicates, although zeolite rho, in both its aluminosilicate and nonaluminosilicate modifications,[31] shows a rather similar, large, "window-squashing" distortion on ion-exchange and/or thermal treatment. Other studies have shown that zincophosphate and zincoarsenate frameworks are typically less stable to thermal dehydration or ion-exchange than aluminosilicates or aluminophosphates. For instance, hydrated zeolite-X type sodium zincophosphate collapses on dehydration,[4] and sodalite-type $Na_3(ZnAsO_4)_3 \cdot 4H_2O$ reversibly transforms, via Zn−O−As bond-breaking/bond-making, to a hexagonal phase[32] on dehydration. Thus, for example, the ~600 °C thermal stability of $Cs_3Zn_4O(AsO_4)_3 \cdot 4H_2O$ (vide supra) represents one of the most stable types of zincoarsenate framework and may even be rugged enough to allow for possible technological applications.

We have developed starting crystallographic models for the frameworks of the tetragonal form of $Rb_3Zn_4O(PO_4)_3 \cdot 3.5H_2O$ (space group $P\bar{4}c2$) and rhombohedral $Li_3Zn_4O(PO_4)_3 \cdot 6H_2O$ (space group $R3c$), but the excessive number of atomic parameters and inherent high framework pseudosymmetry in these distorted structures led to difficulties in refining these structural models against powder X-ray data. We plan to collect powder neutron data for hydrated and dehydrated modifications of these materials and obtain detailed structural information on framework distortions and guest cation sitings, which will be reported later.

In summing up, we note that the $M_3Zn_4O(XO_4)_3 \cdot nH_2O$ family of phases are a significant addition to the remarkable variety of phases already found as a result of mild-condition (T > 70 °C, ambient pressure) solution-phase preparations in the Na/Zn/P/O system.[10] As with aluminosilicate zeolite syntheses, careful control of pH, concentrations, and reaction times is the key to preparing new phases in this phase space. Table 8 summarizes the pH-dependent structural chemistry of the Na/Zn/P/O phase space, as determined so far. All the reactions may be formulated as

$$Zn(NO_3)_2(aq) + Na_xH_{3-x}PO_4(aq) \xrightarrow{\Delta} Na/Zn/P/O(s)$$

where the reaction temperature varies from below ambient to 70 °C. To be noticed is the fact that at low pH, the structures contain more "acidic" groups, and as the pH increases, more basic elements and groups tend to predominate.

Supporting Information Available: Table of anisotropic thermal factors (1 page); table of observed and calculated structure factors for $Na_3Zn_4O(PO_4)_3 \cdot 6H_2O$ (5 pages). Ordering information is given on any current masthead page.

Acknowledgment. The authors wish to thank E. M. Flanigen for helpful discussions. An anonymous referee made helpful comments concerning the Rietveld refinements. We thank Scott Weigel (UCSB) for carrying out the TGA measurements and Vojislav Srdanov (UCSB) for facilitating the PSHG measurements. Low-temperature single-crystal X-ray data for $Na_3Zn_4O(PO_4)_3 \cdot 6H_2O$ were collected courtesy of Siemens Inc. (Madison, WI). The National Science Foundation (Division of Materials Research) provided partial financial support for this work.

CM950341P

(31) Parise, J. B.; Corbin, D. R.; Gier, T. E.; Harlow, R. L.; Abrams, L.; Von Dreele, R. B. *Zeolites* **1992**, *12*, 360.
(32) Nenoff, T. M.; Harrison, W. T. A.; Newsam, J. M.; Stucky, G. D. *Zeolites* **1993**, *13*, 506.
(33) Whitaker, A. *Acta Crystallogr.* **1975**, *B31*, 2026.
(34) Harrison, W. T. A.; Nenoff, T. M.; Gier, T. E.; Stucky, G. D. *J. Solid State Chem.* **1994**, *113*, 168.
(35) Harrison, W. T. A.; Nenoff, T. M.; Gier, T. E.; Stucky, G. D. *Inorg. Chem.* **1993**, *32*, 2437.
(36) Von Schnering, H.-G.; Nesper, R.; Stoilova, D. *Z. Anorg. Allg. Chem.* **1986**, *536*, 137.